

Estimation of microstructural properties from synchrotron X-ray microtomography and determination of the REV in paper materials

S. Rolland du Roscoat ^{a,b}, M. Decain ^{c,a}, X. Thibault ^b, C. Geindreau ^{c,*}, J.-F. Bloch ^{a,*}

^a *Laboratoire de Génie des Procédés Papetiers (LGP2), Ecole Française de Papeterie de Grenoble, Institut National Polytechnique de Grenoble, 38000 Grenoble Cedex, France*

^b *European Synchrotron Radiation Facility, 6 Rue Jules Horowitz, Polygone Scientifique, BP220, 38043 Grenoble, France*

^c *Laboratoire Sols-Solides-Structures (3S), CNRS, Universités de Grenoble (INPG-UJF), BP53, 38041 Grenoble Cedex, France*

Received 10 June 2006; received in revised form 27 November 2006; accepted 29 November 2006

Available online 26 February 2007

Abstract

The porosity and specific surface areas of four industrial paper materials were determined from synchrotron X-ray microtomography. The porosity profile within the thickness of each paper material shows that a paper sheet consists of three layers: two boundary layers, which present a strong gradient of porosity, and a “bulk” layer in which the porosity is almost constant. The anisotropy and the heterogeneity scale of the microstructure in the “bulk” layer was then analyzed by means of covariograms. It is shown that the microstructure of the four studied papers is transverse isotropic and that the anisotropy of papers containing fillers is less pronounced. Finally, the representative elementary volume (REV) for both studied microstructural properties was evaluated using two techniques: a systematic analysis of the influence of the volume size on the property measurement, and a statistical methodology. The REVs given by both methodologies are then compared.

© 2007 Acta Materialia Inc. Published by Elsevier Ltd. All rights reserved.

Keywords: Microstructure; Synchrotron X-ray tomography; Image analysis; Porous material; Fibers

1. Introduction

The overall physical properties of heterogeneous materials depend on their microstructure and the intrinsic properties of each constituent. When the variation in the properties of the constituents is small, overall properties can often be estimated or bounded accurately if the volume fractions of each constituent are known [1–3]. When the variation in the constituent properties is high, as in the case of porous or fibrous material, the overall properties of the material obviously depend on the pore (or solid) volume fraction ϕ , but also on other morphological properties such as the specific surface area S (m^{-1}). For example, the permeability

K (m^2) for an isotropic porous medium is usually expressed as $K = \phi/(c S^2)$, where c is a constant [4]. The study of these interactions between physical phenomena and microstructure and their effect on the overall properties of heterogeneous materials has been the subject of much research. This is also the main goal of all homogenization theories (or upscaling techniques) [2,3,5] which aim at describing heterogeneous material in terms of macroscopic homogeneous properties. To this end, macroscopic behavior is derived from the description at the heterogeneity scale that describes the physical process over a representative elementary volume (REV). By definition, the REV is large enough to represent the heterogeneity scale, and small compared to the macroscopic volume. This fundamental condition of separation of scales is expressed as $l \ll L$, where l and L are the characteristic lengths at the REV and at the macroscopic scale, respectively. This definition intuitively suggests a geometrical separation of scales, but

* Corresponding authors. Tel.: +33 4 76 82 51 76; fax: +33 4 76 82 70 43 (C. Geindreau), tel.: +33 4 76 82 69 71 (J.-F. Bloch).

E-mail addresses: christian.geindreau@hmg.inpg.fr (C. Geindreau), jean-francis.bloch@epfg.inpg.fr (J.-F. Bloch).

this fundamental condition must also be verified regarding the excitation, i.e. the physical phenomenon under consideration [5–8].

Much analytical and numerical work has been done to determine the effective properties of a composite material with well-defined microstructure (periodic or random) [7–9]. In the last 15 years, it has become possible to perform large computations [4,8,10–14] for calculating the properties of real three-dimensional (3-D) microstructures obtained by using 3-D imaging techniques (synchrotron X-ray microtomography, confocal microscopy, etc.). One difficulty with this approach is directly linked to the size of the 3-D microstructure images which are often limited. Therefore, is it possible to determine a REV? In practice, the REV is often estimated by performing a systematic analysis of the volume size influence on the overall geometrical and physical properties [11,13]. This “deterministic” REV is given by the size of the volume for which the fluctuations of the effective property become limited. In order to overcome the above difficulties, numerical and statistical computational homogenization methodologies have been proposed [7,8,13]. In Ref. [13], the porosity, the specific surface area and the permeability of sintered crushed glass beads and Brent Tiassic sandstone were computed by moving a cubic window of different scales centered at various locations through the sample. Then, for a given size of the cubic window, the mean value of each property and their standard deviation were estimated. From these results, the authors defined the statistical REV as the size of a volume beyond which the mean of the effective studied quantity becomes approximatively constant, and the coefficient of variation, defined as the ratio between the standard deviation and the mean, is less than a given value (20% for example). This REV also depends on the number of realizations. However, this number is not discussed in Ref. [13]. A complete definition of the “statistical” REV has been recently proposed [7,8]. In these works, it is shown that the effective physical properties of heterogeneous materials can be determined not only by one numerical simulation on a REV, but also as the mean values of apparent properties of volumes smaller than the REV, provided that a sufficient number of realizations of the microstructure are considered. Consequently, the “statistical” REV is defined as a function of the physical properties of each constituent, their contrast, the microstructure, the desired precision and the number of realizations. This methodology was applied to determine the REV for linear elastic and thermal properties of specific random microstructures [7] and of real microstructures of materials from the food industry [8].

The aim of this paper is to measure the microstructural properties, such as the porosity and the specific surface area, of four different industrial paper materials and to determine the corresponding REV. Such knowledge is important for future computations of the effective physical properties (permeability, thermal conductivity, etc.) and for future development of the functional properties of such material. The four paper materials studied are presented

in Section 2. The microstructural properties studied in this work were computed from 3-D images obtained by synchrotron X-ray microtomography. The acquisition of these images and their treatment are presented in Section 3. The methods used to measure the porosity and the specific surface area of the samples are presented in Section 4. Since the porosity is heterogeneous within the thickness of our sample, all the measurements presented in this work were performed on volume with a limited thickness located in the “bulk” part of the paper. The size of this “bulk” layer and the anisotropy of the microstructure is then discussed. Section 5 is devoted to the determination of the volume size of our materials which is representative of the porosity or the specific surface area. For this purpose, the influence of the volume size on the microstructural properties measurements is analyzed. From these results, the “deterministic” REV is estimated. Finally, following the methodology presented in Refs. [7,8], the “statistical” REV for the porosity is determined and compared to the previous finding.

2. Materials

Paper is essentially made of cellulose fibers. During production of wood fiber-based products, the fibrous water suspension (99% water) is basically laid down on a fabric, pressed and dried. At the end of the process, the amount of water in the consolidated structure is less than 5%. Depending on the required final properties, different types of fibers may be used. The two main types of fibers are softwood (spruce, pine, etc.) and hardwood (birch, eucalyptus, etc.). Hardwood fibers are typically 20 μm in diameter and about 1 mm long, whereas softwood fibers are 40 μm in diameter and 3 mm long. In many papers, fillers (up to 40% of mass) are added in order to improve optical properties. Fillers are mineral particles such as CaCO_3 (GCC: natural ground, or PCC: precipitated), clay or TiO_2 . They differ in terms of shapes and sizes. The sizes of the particles are typically 20, 2, 20 and 0.3 μm for GCC, PCC, clay and TiO_2 , respectively. In order to cover a broad range of paper grades, properties and applications, four papers are considered:

- Paper “hard”: this is a hand sheet (a laboratory-made paper) made entirely of hard-wood fibers. The paper-making process is static: the sheet is formed on a grid by suction, giving the sample a naturally isotropic structure within the plane of the paper sheet. No special characteristics were sought; it was mainly a test hand sheet.
- Paper “blot”: this is an industrial blotting paper. It is made on a pilot paper machine, at slow speed (2 m s^{-1}), from a mix of softwood and hardwood fibers, with no added fillers. The required property of this type of paper is the absorption capacity with regards to strength under humidity.
- Paper “deco”: this is an industrial decorative paper used for structural applications. It is also made of a mix of softwood and hardwood fibers, and filled with 35–40%

of TiO_2 . It is produced at moderate speed (10 m s^{-1}) on an industrial paper machine. The required property of this paper is strength under mechanical stress.

- Paper “copy”: this is a common industrial printing paper. It contains different fibers (softwood, hardwood, recycled, etc.) and fillers (around 20% of precipitated CaCO_3). It is produced at high speed (25 m s^{-1}) on an industrial paper machine. This kind of paper must satisfy several properties: strength under thermal and mechanical stresses, opacity, brightness, etc.

Table 1 presents the main characteristics of these samples. The grammage G (g m^{-2}) and the thickness e (μm) were measured using standards. From these two quantities, we can estimate the porosity ϕ_m defined as

$$\phi_m = 1 - G/(e\rho), \quad (1)$$

where ρ is the density of the paper. This density is written, $\rho = x\rho_c + (1 - x)\rho_a$, where x is the mass fraction of fillers, $\rho_c = 1540 \text{ kg m}^{-3}$ is the cellulose density and ρ_a is the density of fillers: $\rho_a = 2700 \text{ kg m}^{-3}$ and $\rho_a = 4000 \text{ kg m}^{-3}$ for the CaCO_3 and the TiO_2 , respectively. The porosity of

the studied papers varies between 0.43 for “copy” and 0.66 for “blot”.

3. Image acquisition and treatment

The work presented in this paper was carried out on images of various paper samples acquired by synchrotron X-ray microtomography. This technique gives access to the 3-D structure of the samples in a non-destructive way [15]. All the data presented in this work were acquired on the ID19 beamline of the European Synchrotron Radiation Facility (ESRF), Grenoble, France. According to the fiber dimensions, a pixel size of $0.7 \mu\text{m}$ was chosen leading to a volume imaged of $(1400 \times 1400 \times e \mu\text{m}^3)$, i.e. $(2048 \times 2048 \times e/0.7 \text{ voxels})$. The size of samples is limited in the z direction which corresponds to the paper thickness e . To obtain quantitative parameters on the structure, the two main phases of the paper samples, i.e. the pore phase and the solid phase that consists of fibers and fillers, are separated. This is performed by using segmentation tools dedicated to paper images acquired by this technique [16]. During the paper-making process, fillers (TiO_2) may agglomerate to form clusters of about $5 \mu\text{m}$. Consequently, these fillers (TiO_2) contained in the paper “deco” can be visualized with the chosen resolution.

Fig. 1 presents 3-D visualizations of the four paper samples. This figure shows that most of the fibers are in the plane (x, y) . Thus, these microstructures seem to be mainly orthotropic. Moreover the paper “hard”, which contains hardwood fibers, only seems to be homogeneous. On the 3-D images of the “blot” and “copy” samples, we can distinguish the hardwood fibers (small fibers) and the softwood fibers (large fibers) present in these papers. Due to the large amount of fillers in the paper “deco”, it is more

Table 1
Grammage G , thickness e , mass fraction of fillers x measured on the different papers

	‘Hard’	‘Blot’	‘Deco’	‘Copy’
G (g/m^2)	67	246	85	80
e (μm)	109	473	97	111
x (%)	0	0	40	20
ϕ_m	0.6	0.66	0.43	0.59

The porosity ϕ_m is given by the relation (1).

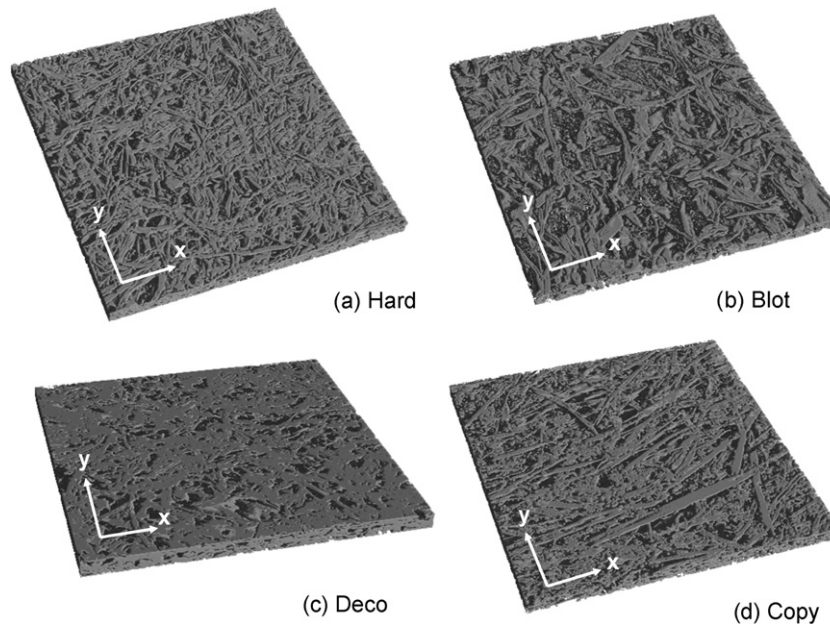


Fig. 1. 3-D visualization of the four paper samples. The size of each sample is $(700 \times 700 \times 35 \mu\text{m}^3)$.

difficult to distinguish the fibers. The microstructure of the paper “deco” seems to be less orthotropic than the others. Finally, we can observe that the paper “blot” and the paper “deco” appear as the most porous paper and the least porous paper, respectively. These observations are in agreement with our measurements presented in Section 2 and reported in Table 1.

4. Microstructural properties measurements: methods and limitation

4.1. Porosity and specific surface area measurements

The porosity is evaluated from the binarized volume as the ratio of the voxels belonging to the pore phase, to the whole number of voxels in the volume. The specific surface area, defined as the ratio of the total interstitial surface area to the bulk volume, is estimated by stereology measurement using the Saltikov relation [17,18]. This relation links S (m^{-1}) to the mean intercept number per unit of length $\langle P \rangle$ in all the directions of the space through the relation: $S = 2\langle P \rangle$. In the following, all the results of the specific surface area are presented in dimensionless form: $S^* = (S/S_c)$, where the characteristic specific surface area S_c has been arbitrarily chosen to be equal to $1.2 \times 10^5 \text{ m}^{-1}$.

4.2. Porosity profile within the thickness

The above measurements were carried out on volumes ($l \times l \times h \text{ } \mu\text{m}^3$) where the size h along z is obviously smaller than the paper thickness e . Moreover, the microstructural properties of a sheet of paper are heterogeneous within the thickness. Fig. 2 shows the evolution of the porosity vs. the dimensionless thickness z/e for the different paper materials. The porosity presented on this figure is measured from the whole sections ($1000 \times 1000 \text{ } \mu\text{m}^2$) perpendicular

to the z axis of the samples. We observe that the porosity is not constant throughout the thickness of the paper. These porosity profiles are similar to those already measured in fibreboards [19]. The porosity profiles of papers “hard”, “blot” and “copy” are almost symmetric. By contrast, the porosity profile of the paper “deco” is non-symmetric. Such symmetry (or non-symmetry) of the porosity profile is controlled during the paper-making process. In the boundary layers, a strong porosity gradient is present. The thickness of these boundary layers is equal to 50% and 70% of the total thickness for the papers “hard”, “blot” and “copy”, and for the paper “deco”, respectively. It is clear that such a porosity gradient, which is a microstructural property, plays an important role in many properties of paper sheets. Unfortunately, the measurement of this gradient is currently biased for two reasons: the top and the bottom ($z/e = 0$ or 1) surfaces of the samples are not completely flat or may be slightly inclined with respect to the z axis during the image acquisition. Nevertheless, in the “bulk” layer (between a and b in Fig. 2), the porosity of each paper is almost constant, and therefore not biased by the experimental conditions.

The mean value of the porosity ϕ_b in the “bulk” layer and its standard deviation σ_b are reported in Table 2. The mean values of the porosity ϕ_t throughout the thickness ($0 < z/e < 1$) were also computed for each paper and are reported in Table 2. The porosity ϕ_t may be compared with the measured porosity ϕ_m (Table 1). The difference between these two quantities may vary between 2% for the paper “copy” and 14% for the paper “blot”. These discrepancies are mainly due to the inaccuracy of the measurements of the boundary layers. In the following, we will focus our study on the microstructural properties of the different papers in the “bulk” layer only. Thus, the porosity ϕ_b and the dimensionless specific surface area S_b^* computed for the whole “bulk” layer and presented in Table 2 will be used as reference in what follows.

4.3. Anisotropy

Fig. 1 clearly shows that most of the fibers are in the plane (x, y) and that the microstructure of each paper seems

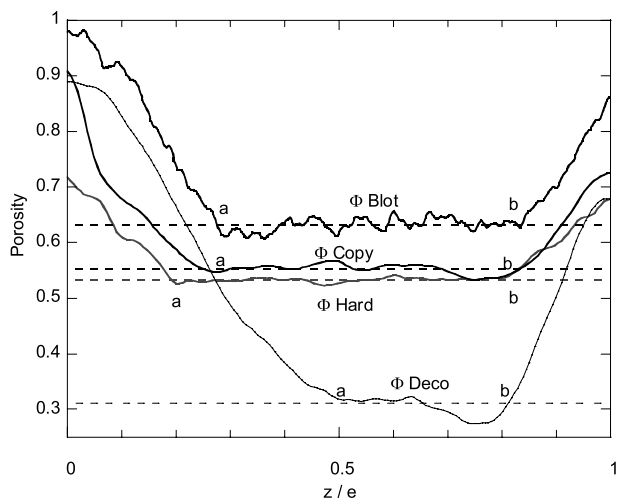


Fig. 2. Evolution of the porosity vs. the dimensionless thickness z/e for the different papers. Dashed lines represent the mean porosity ϕ_b in the “bulk” layer (between a and b) for each paper.

Table 2

ϕ_b is the mean porosity in the “bulk” layer, σ_b is the standard deviation of ϕ_b estimated for a volume ($1000 \times 1000 \times 0.5 e \text{ } \mu\text{m}^3$), ϕ_t is the mean porosity within the whole thickness, S_b^* is the mean value of the dimensionless specific surface area in the “bulk” layer, l_x , l_y and l_z are the covariance ranges along x , y and z , respectively

	‘Hard’	‘Blot’	‘Deco’	‘Copy’
ϕ_b	0.53	0.64	0.31	0.54
σ_b	0.004	0.012	0.022	0.009
ϕ_t	0.57	0.71	0.49	0.6
$S_b^* = S_b/S_c$	0.91	0.78	0.57	0.82
$l_y = l_x$ (μm)	33	26	31	20
l_z (μm)	2.5	3.5	5.5	4.5
l_x/l_z	12.4	7.4	6	4.4

to be orthotropic, as already mentioned. In order to verify this hypothesis, we determined the covariance along x , y and z from images of plane sections of our samples [20,21]. The covariance function of the set X is the probability that the two points x and $x + h$ be in the set X . Fig. 3 shows the covariances along the x , y and z directions for the paper “hard”. Similar diagrams were obtained for the other paper samples. We can observe that the covariances are equal in both the x and y directions. Thus, the microstructure is isotropic within the plane (x, y). However, the covariance along z differs from the other two directions. Therefore the 3-D microstructure is transverse isotropic. These covariances reach an asymptotic value equal to the square of the porosity for a finite range $lc_x = lc_y$ or lc_z . These lengths characterize the size of heterogeneities in a given direction. The covariance ranges lc_x (or lc_y) and lc_z of each paper are summarized in Table 2. The characteristic size of heterogeneities lc_x (or lc_y) within the plane (x, y) for the different papers are of the same order of magnitude as the fiber diameter, i.e. around $30 \mu\text{m}$. The covariance range lc_z is much smaller than lc_x (or lc_y). The ratio lc_x/lc_z characterizes the anisotropy of the microstructure. This ratio varies between 4.4 for the paper “copy” and 12.4 for the paper “hard” (Table 2). As expected, these results show that the anisotropy of the “copy” and “deco” papers is less pronounced due to the presence of fillers. Finally, we can remark in Fig. 3 that the covariance curves slightly decrease with increasing length and go below their sill. In order to determine a possible characteristic length larger than $lc_x = lc_y$ or lc_z , we have computed the covariance

along x , y and z from the largest images, typically ($1000 \times 1000 \mu\text{m}^2$) and ($1000 \times 0.5 e \mu\text{m}^2$). The obtained results showed that the studied microstructures do not exhibit another characteristic length in these ranges.

5. Determination of the REV in the “bulk” layer

The aim of this last section is to determine the REV for both the porosity and the specific surface area in the “bulk” layer. Such knowledge is important for future computations of the physical effective properties (permeability, thermal conductivity, etc.) of the paper materials. In the following, the REV is determined by following either a “deterministic” or a “statistical” approach.

5.1. “Deterministic” REV quantification

In order to determine the “deterministic” REV of the samples, we have first performed a systematic analysis of the influence on the porosity and specific surface area of the volume size ($l \times l \times h \mu\text{m}^3$), when the size h along z is kept constant and equal to $35 \mu\text{m}$. This size has been chosen as it corresponds to the maximal thickness of the “bulk” layer of the paper “deco” (Fig. 2). Figs. 4 and 5 present the evolution of the porosity and the dimensionless specific surface area of the different paper samples vs. the size l , respectively. The size l varies between $21 \mu\text{m}$ and $700 \mu\text{m}$. On these figures, we have also plotted the mean values ϕ_b and S_b^* (dashed lines) of the porosity and the specific surface area of the whole “bulk” layer (Table 2). These

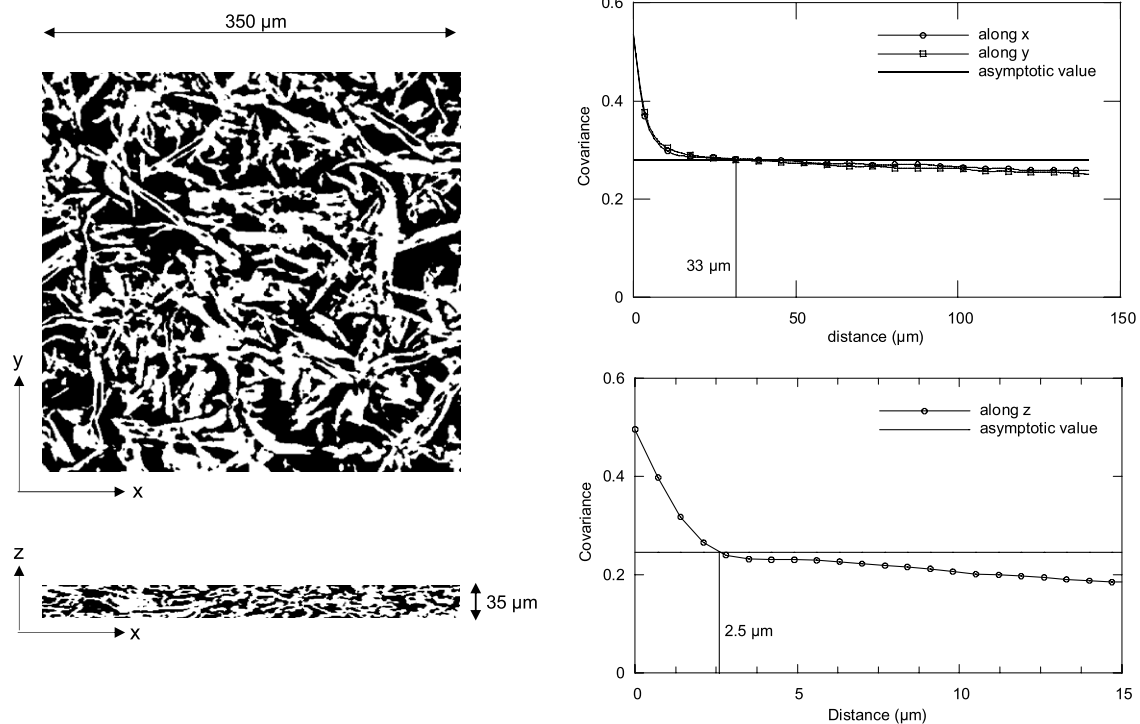


Fig. 3. Paper “hard”: plane sections of the microstructure (pore = black phase) and their covariances along x , y and z directions. The asymptotic value is equal to the square of the porosity.

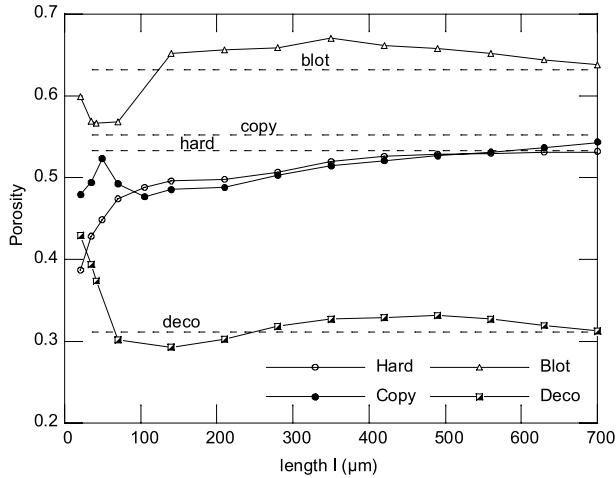


Fig. 4. Evolution of the porosity ϕ vs. the size l of the volume ($l \times l \times 35 \mu\text{m}^3$) for the different papers. Dashed lines represent the mean porosity ϕ_b in the “bulk” layer for each paper.

figures show that both properties become more or less stable and tend towards mean values ϕ_b and S_b^* while l increases.

We next performed a systematic analysis of the influence on the porosity and the specific surface area of the volume size ($l \times l \times h \mu\text{m}^3$) when the thickness h varies between 0 and $35 \mu\text{m}$ and the size l is kept constant. Fig. 6 presents the evolution of the porosity and the dimensionless specific surface area of the paper “hard” vs. the thickness h of the volume and for several values of l between 35 and $700 \mu\text{m}$. This figure shows that for a given length $l > 70 \mu\text{m}$, both properties reach a constant value when h is larger than $20 \mu\text{m}$. Similar results were obtained for the other paper samples.

These analyses indicated that both properties of the paper materials mainly depend on the size l of the volume in the plane (x, y). This result is directly linked to the characteristic length of the heterogeneities lc_x (or lc_y) within the plane (x, y), which are much larger than lc_z . The “determin-

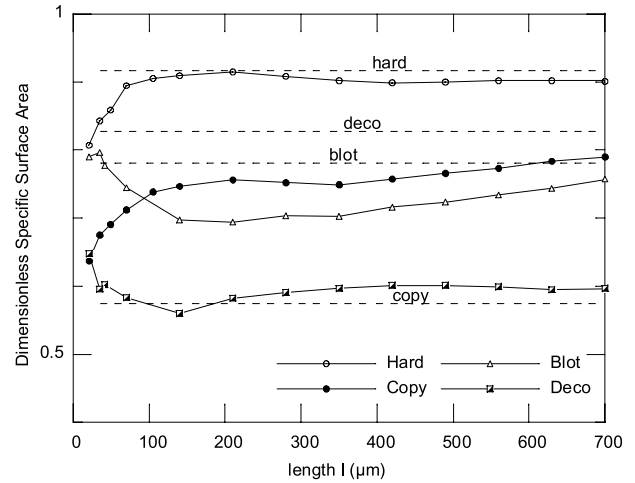


Fig. 5. Evolution of the dimensionless specific surface area S^* vs. the size l of the volume ($l \times l \times 35 \mu\text{m}^3$) for the different papers. Dashed lines represent the mean specific surface area S_b^* in the “bulk” layer.

istic” REV l of the paper samples appears to be proportional to the length of the heterogeneities: $l = N \times lc_x$, where N may be viewed as the “number of heterogeneities”. From Figs. 4 and 5 we have computed the relative errors $(\phi - \phi_b)/\phi_b$ and $(S^* - S_b^*)/S_b^*$ for $N = 10$. In order to test the sensitivity of this parameter, we have also computed these errors for $N = 20$. These errors are reported in Table 3. When $N = 10$, the relative error for the porosity is lower than 5% for the papers ‘hard’, ‘blot’ and ‘deco’, and larger than 10% for the paper ‘copy’. The relative error $(S^* - S_b^*)/S_b^*$ for the dimensionless specific area varies between 1.3% for the paper ‘hard’ to 9.9% for the paper ‘blot’. As expected, these errors decrease with increasing N , i.e the length l . When $N = 20$, both errors for the different papers are lower than 5%.

5.2. “Statistical” REV quantification

In order to determine the “statistical” REV for both the porosity and the specific surface area of the samples, we

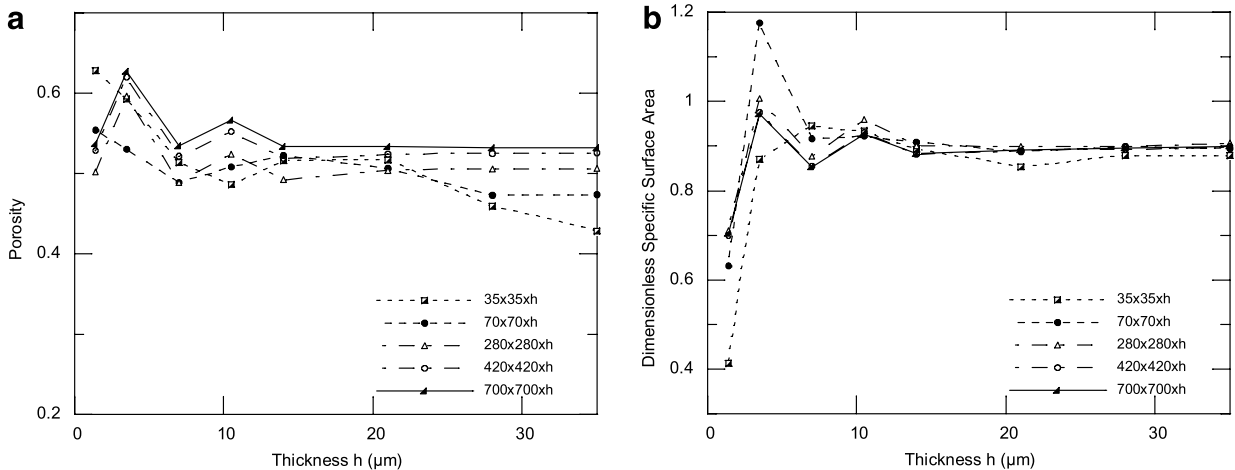


Fig. 6. Paper “hard”. Evolution of the porosity ϕ (a) and the dimensionless specific surface area S^* (b) vs. the thickness h of the volume ($l \times l \times h \mu\text{m}^3$) and several values of l between $35 \mu\text{m}$ and $700 \mu\text{m}$.

Table 3

Relative errors $(\phi - \phi_b)/\phi_b$ and $(S^* - S_b^*)/S_b^*$ for a volume size $(l \times l \times 35 \mu\text{m}^3)$ with $l = N \times l_{c_x}$ ($N = 10$ or 20)

Size	Errors (%)	'Hard'	'Blot'	'Deco'	'Copy'
$l = 10 \times l_{c_x}$	$(\phi - \phi_b)/\phi_b$	3.6	4.3	5	11.6
$l = 10 \times l_{c_x}$	$(S^* - S_b^*)/S_b^*$	1.3	9.9	3.8	8.5
$l = 20 \times l_{c_x}$	$(\phi - \phi_b)/\phi_b$	0.3	3.1	2.3	5.6
$l = 20 \times l_{c_x}$	$(S^* - S_b^*)/S_b^*$	1.6	4.8	3.5	5.0

have computed the porosity $\phi_i(V)$ and the dimensionless specific surface area $S_i^*(V)$ of five non-overlapping sub-volumes P_i arbitrarily located in the sample. The sub-volume size is $V = (l \times l \times 35 \mu\text{m}^3)$ where l varies within the range 21–210 μm . Figs. 7 and 8 show the evolution of $\phi_i(V)$ and $S_i^*(V)$ vs. the size l of sub-volume, respectively. The results of the sub-volume P_1 correspond to those already presented in Figs. 4 and 5. In Figs. 7 and 8, we have also plotted the average values $\bar{\phi}(V)$ and $\bar{S}^*(V)$ of the porosity $\phi_i(V)$ and the dimensionless specific surface area $S_i^*(V)$ vs. the size l of sub-volume V , respectively. These figures suggest the following comments: (i) as expected, the porosity $\phi_i(V)$ and the specific surface $S_i^*(V)$ of a given sub-volume

P_i tend towards the mean values ϕ_b and S_b^* , increasing the size l of the sub-volume; (ii) the dispersion of the results decreases with increasing sub-volume size; and (iii) the average values $\bar{\phi}(V)$ and $\bar{S}^*(V)$ tend rapidly (for $l < 100 \mu\text{m} = 3\text{--}4$ times l_{c_x}) towards the mean values ϕ_b and S_b^* . These tendencies are similar to those already observed for the microstructural properties (porosity and specific surface area) of sandstone [13] and also for the effective properties (thermal conductivity and elasticity) of different materials [7,8].

As in Refs. [7,8], these results suggest that the effective microstructural properties of the paper samples may be estimated from the mean values of the apparent properties of volumes smaller than the “deterministic” REV, provided that a sufficient number of realizations of the microstructure is considered. In Refs. [7,8], the authors defined the “statistical” REV as a function of the physical properties of each constituent, their contrast, the microstructure, the required precision and the number of realizations. This “statistical” REV is based on the notion of the integral range A_3 , which depends on the studied property. The integral range is linked to the scatter in apparent

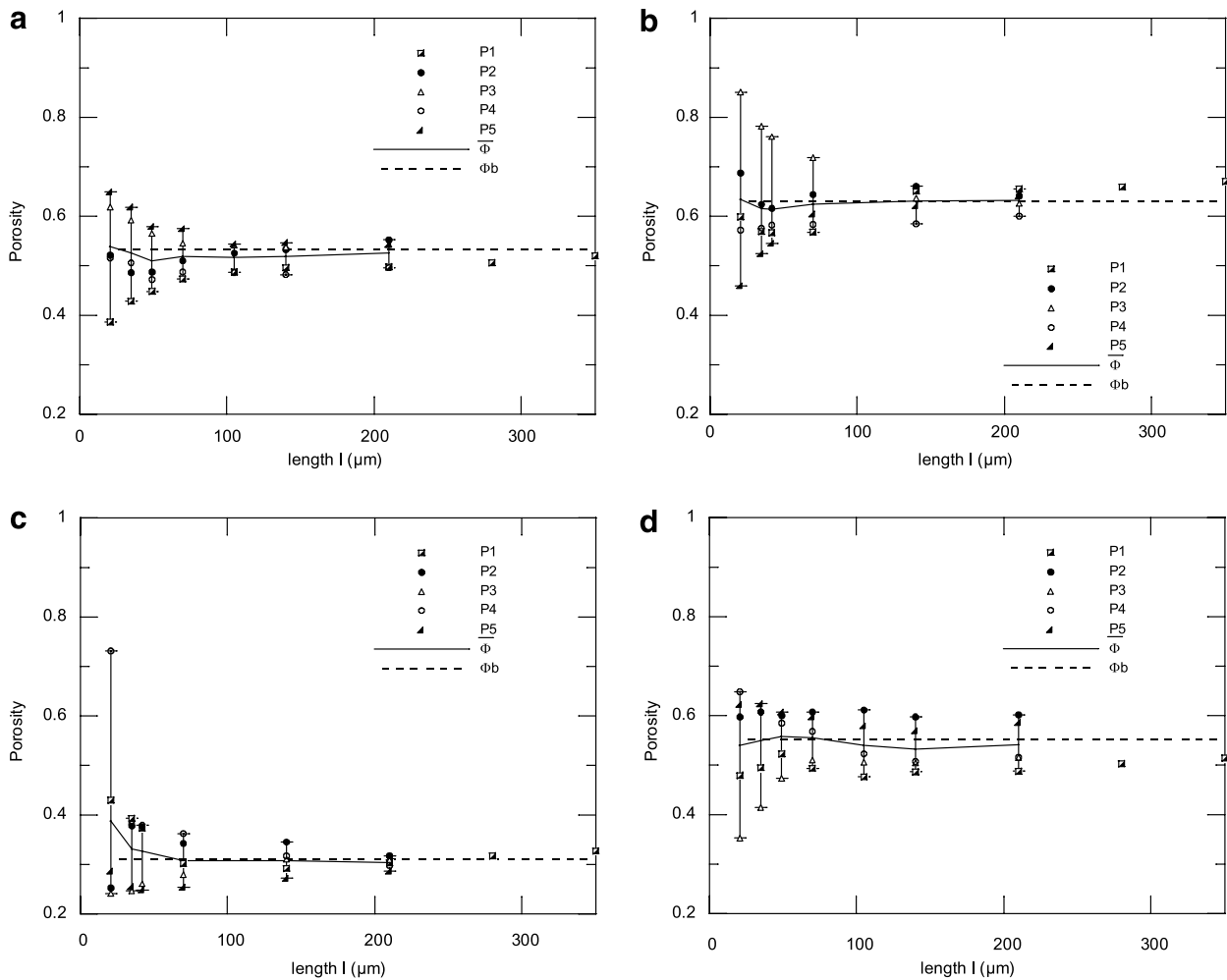


Fig. 7. Evolution of the porosity $\phi_i(V)$ of the sub-volume P_i vs. the size l of sub-volume $V = (l \times l \times 35 \mu\text{m}^3)$. The continuous line represents the average value $\bar{\phi}(V)$ of $\phi_i(V)$. The dashed line represents the mean value ϕ_b . (a) Paper “hard”, (b) paper “blot”, (c) paper “copy” (d) paper “deco”.

properties found on sub-volumes of fixed size V but containing several realizations n of the microstructure. For the porosity, we have (see Refs. [7,8] for details):

$$D_\phi^2(V) = \phi_b(1 - \phi_b) \frac{A_3}{V} \quad (2)$$

where $D_\phi^2(V)$ is the variance of the porosity evaluated for sub-volumes of size V . It can be shown [7,8] that the smallest volume necessary and sufficient to estimate the porosity with a given relative error ε and number n of realizations may be written as:

$$V(n, \varepsilon) = 4 \frac{(1 - \phi_b)}{\phi_b} \frac{A_3}{n\varepsilon^2} \quad (3)$$

The extension of relations (1) and (2) for the specific surface area is not straightforward and is not considered in the following. In order to determine the integral range A_3 , from data presented in Fig. 4 we have computed the variance $D_\phi^2(V)$ of the porosity evaluated for sub-volumes of size V . Fig. 9 shows the evolution of $D_\phi^2(V)$ vs. the sub-volume size V (or l) for the different papers. Finally,

the integral range A_3 for the porosity is obtained by fitting the relation (1) on these data (continuous line in Fig. 9). The values of A_3 adjusted in our data are summarized in Table 4. One can now define the minimum “statistical” REV l , for a given relative error and number of realizations. In order to compare both “deterministic” and “statistical” approaches, we have computed the “statistical” REV of each paper for $n = 1$ and $n = 5$, and for the same relative error reported in Table 4 for the “deterministic” REV when $l = 10 \times lc_x$ ($N = 10$). The obtained results are summarized in Table 4. When $n = 1$, the “statistical” REV predicted by the model (2) for papers “hard”, “blot” and “deco” is of the order of $8\text{--}10 \times lc_x$. This size is of the same order of magnitude as the “deterministic” one ($10 \times lc_x$) for the same relative error. For the paper “copy”, the “statistical” REV predicted by the model (2) is much smaller than the “deterministic” one. Note that if we consider a relative error of 5% as for the paper “deco”, the “statistical” REV for the paper “copy” given by the model (2) is of the order of $7 \times lc_x$. Consequently, for the same relative error and for $n = 1$, the “statistical” REV of the

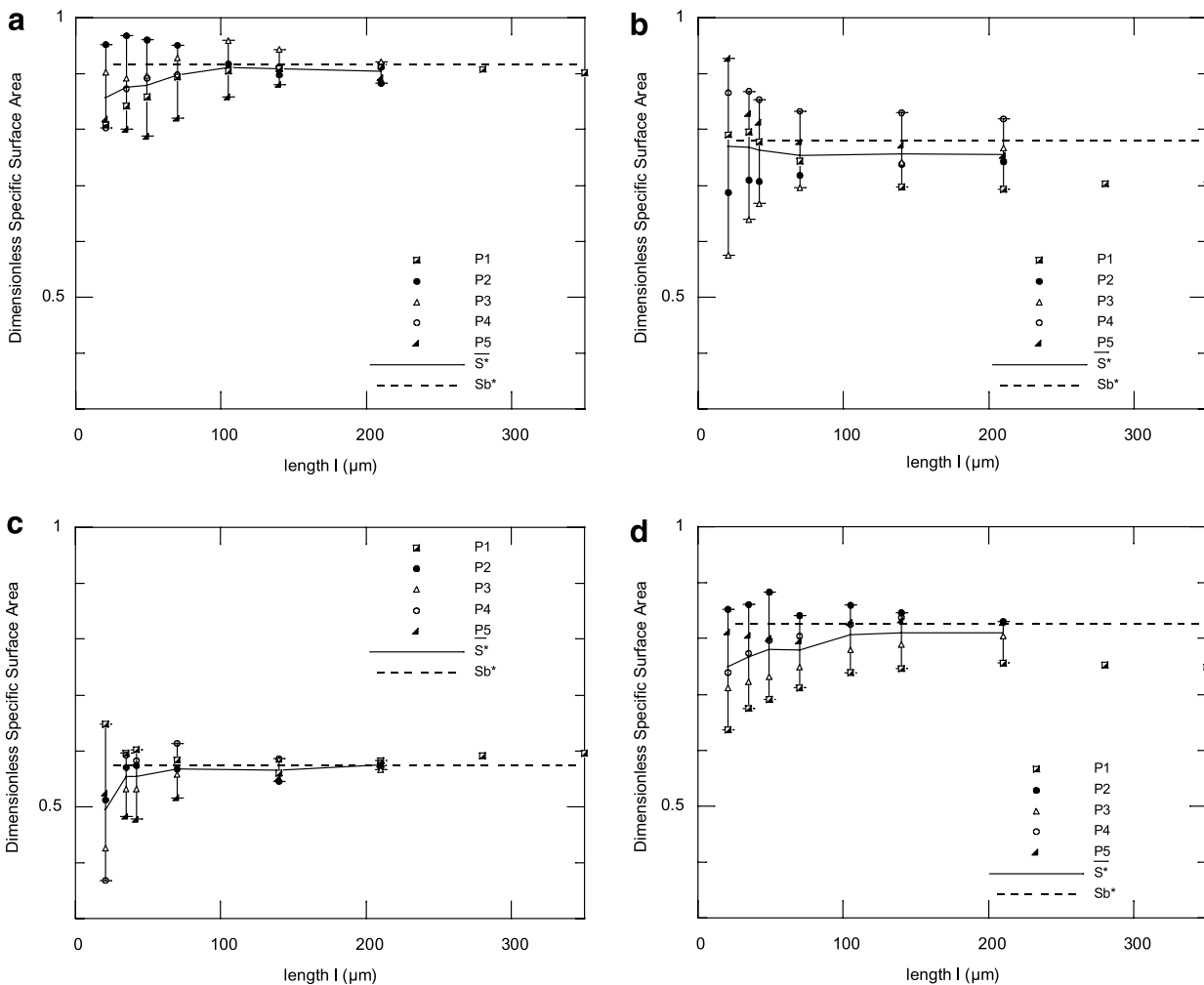


Fig. 8. Evolution of the dimensionless specific area $S_i^*(V)$ of the sub-volume P_i vs. the size l of sub-volume $V = (l \times l \times 35 \mu\text{m}^3)$. The continuous line represents the average value \bar{S}^* of $S_i^*(V)$. The dashed line represents the mean value S_b^* . (a) Paper “hard”, (b) paper “blot”, (c) paper “copy” (d) paper “deco”.

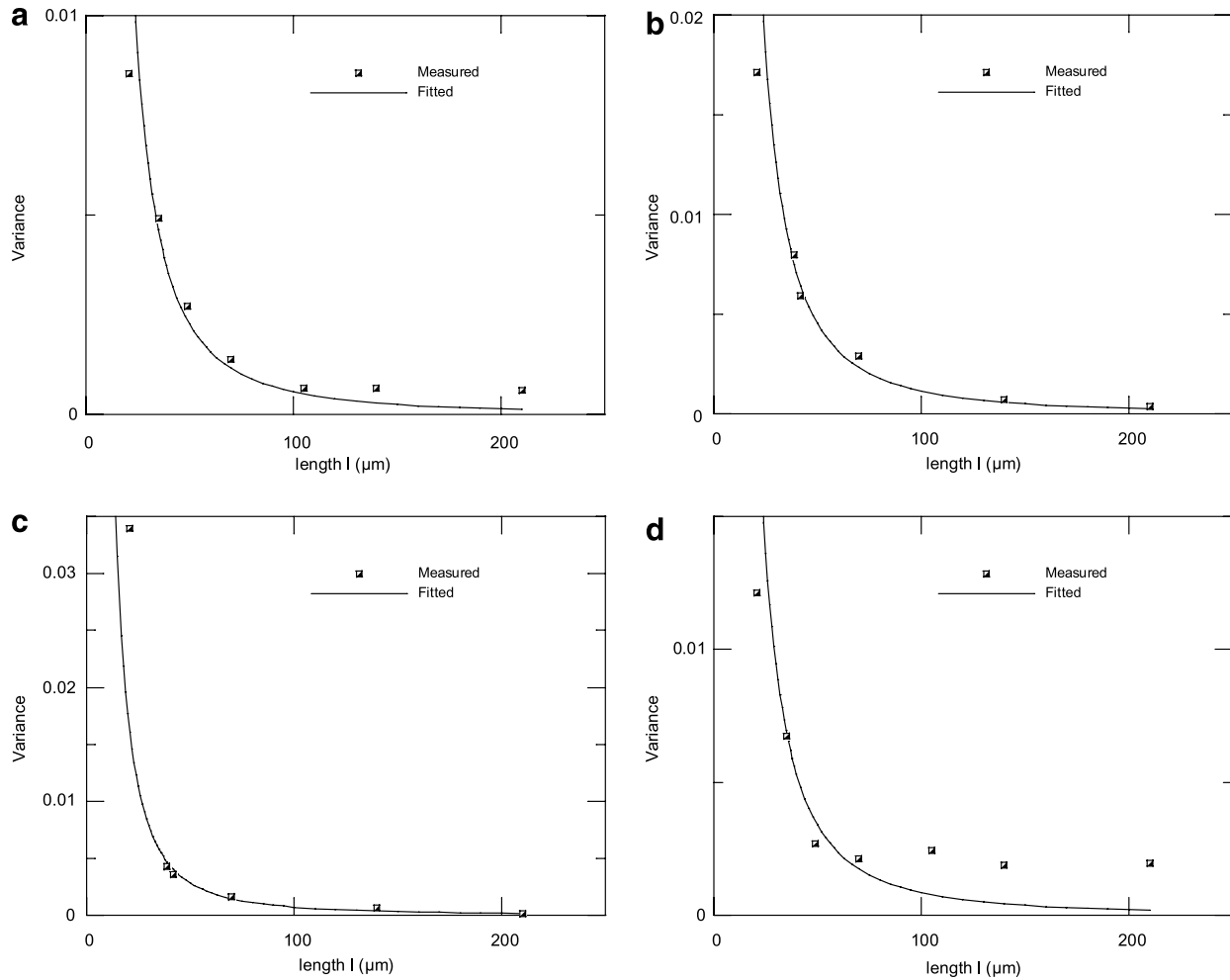


Fig. 9. Evolution of the variance of the porosity $D_{\phi}^2(V)$ vs. the size l of sub-volume $V = (l \times l \times 35 \mu\text{m}^3)$. The continuous line represents the relations (1) fitted on the data (a) paper “hard”, (b) paper “blot”, (c) paper “copy” (d) paper “deco”.

Table 4

Integral range A_3 for the porosity. Estimations of the REV ($l \times l \times 35 \mu\text{m}^3$) for different numbers n of realization and for the same relative error ε presented in Table 3 when $l = 10 \times lc_x$

	‘Hard’	‘Blot’	‘Deco’	‘Copy’
A_3 (μm^3)	800	1600	1000	540
ε (%)	3.6	4.3	5	11.6
$l(\varepsilon, n = 1)$ (μm)	$250 \approx 8 \times lc_x$	$241 \approx 9.2 \times lc_x$	$318 \approx 9.6 \times lc_x$	$61 \approx 3 \times lc_x$
$l(\varepsilon, n = 5)$ (μm)	$111 \approx 3.6 \times lc_x$	$107 \approx 4.1 \times lc_x$	$142 \approx 4.3 \times lc_x$	$27.4 \approx 1.3 \times lc_x$

different papers is of the same order of magnitude. When $n = 5$, the “statistical” REV for the papers “hard”, “blot” and “deco” predicted by the model is now of the order of 3 or $4 \times lc_x$. These results are in agreement with our data on Fig. 4. For the paper copy, the “statistical” REV is still smaller since the selected relative error is larger.

6. Concluding remarks

In this paper, microstructural properties such as the porosity and specific surface area of four different industrial paper materials were computed from synchrotron X-ray microtomography.

From the porosity profile within the thickness, we have shown that a paper sheet is constituted of three layers: two boundary layers, which present a strong gradient of porosity, and a “bulk” layer in which the porosity is almost constant. It is clear that these boundary layers, which represent more than 50% of the total thickness of the paper, play an important role in many properties of a paper sheet. Currently the microstructural properties measurements in these boundary layers are biased by the experimental conditions, and therefore need to be improved.

In order to study the anisotropy of the microstructure in the “bulk” layer of each paper, we have computed the covariogram in the three directions and determined the

corresponding covariance range, which characterizes the heterogeneity scale. From these results, we have shown that (i) the microstructure of all the studied paper materials are transverse isotropic; (ii) the anisotropy of papers containing fillers is less pronounced; (iii) the heterogeneity scale ($lc_x = lc_y$) within the plane of a paper sheet is of the same order of magnitude as the fiber diameter; and (iv) the heterogeneity scale (lc_z) within the thickness is much smaller.

Attention was then focussed on the determination of REV for both the porosity and the specific surface area in the “bulk” layer of each paper. Such knowledge is important for computations of the effective physical properties of paper materials. For this purpose, a systematic analysis of the influence of the REV on the property measurement was first performed. From these results, we have shown that the “deterministic” REV mainly depends on the heterogeneity scale ($lc_x = lc_y$) within the plane (x, y). To a first approximation, a volume size ($l \times l \times h \mu\text{m}^3$) with $h = 35 \mu\text{m}$ and $l = 10 \times lc_x$ seems representative of both the porosity and the specific surface area of all the analyzed paper samples with a relative error of less than 10%. Finally, following the statistical methodology presented in Refs. [7,8], it has been shown that it is possible to estimate the effective microstructural properties of the paper materials from the apparent properties of several volumes smaller than the “deterministic” REV. From the results obtained concerning the porosity, the model proposed in Refs. [7,8] has been fitted. The “statistical” REV predicted by this model depends on the relative error and the number of realizations. For one realization and the same relative error, we showed that the “statistical” REV predicted by the model is of the same order as the “deterministic” one. Based on these results, further work will concern the computation of the effective physical properties (permeability, elastic properties, etc.) of the presented materials.

Acknowledgements

The authors thank their industrial partners: Tembec, Clairefontaine and Arjowiggins, and the “Region Rhône Alpes” of France for the financial support of this work.

References

- [1] Hashin Z, Shtrikman S. A variational approach to the theory of the elastic behavior of multiphase materials. *J Mech Phys Solids* 1963;11:127–40.
- [2] Torquato S. Random heterogeneous materials: microstructure and macroscopic properties. Berlin: Springer Verlag; 2005.
- [3] Milton GW. Theory of composites. Cambridge: Cambridge University Press; 2002.
- [4] Koponen A, Kataja M, Timonen J. Permeability and effective porosity of porous media. *Phys Rev E* 1997;56:3319–25.
- [5] Bornert M, Bretheau T, Gilormini P. Homogénéisation En Mécanique Des Matériaux. Tome 1 et 2. Paris: Hermes; 2001.
- [6] Auriault J-L. Heterogeneous medium. Is an equivalent description possible? *Int J Eng Sci* 1991;29:785–95.
- [7] Kanit T, Forest S, Galliet I, Mounoury V, Jeulin D. Determination of the size of the representative elementary volume element for random composites: statistical en numerical approach. *Int J Solids Struct* 2003;40:3647–79.
- [8] Kanit T, N’Guyen F, Forest S, Jeulin D, Reed M, Singleton S. Apparent and effective physical properties of heterogeneous materials: representativity of samples of two materials from food industry. *Comp Methods Appl Mech Eng* 2006;195:3960–82.
- [9] Idris Z, Orgéas L, Geindreau C, Bloch JF, Auriault JL. Microstructure effects on the flow law of power law fluids through fibrous media. *Model Simul Mater Sci Eng* 2004;12:995–1015.
- [10] Spanne P, Thovert JF, Jacquin CJ, Lindquist WB, Jones KW, Adler PM. Synchrotron computed microtomography of porous media: topology and transports. *Phys Rev Lett* 1994;73:2001–4.
- [11] Bernard D, Gendron D, Heintz J-M, Bordère S, Etourneau J. First direct 3d visualisation of microstructural evolutions during sintering through X-ray computed microtomography. *Acta Mater* 2005;53:121–8.
- [12] Manwart C, Aaltosalmi U, Koponen A, Hilfer R, Timonen J. Lattice-Boltzmann and finite-difference simulations for the permeability for three-dimensional porous media. *Phys Rev E* 2002;66:016702.
- [13] Zhang D, Zhang R, Chen S, Soll WE. Pore scale study of flow in porous media: scale dependency, REV and statistical REV. *Geophys Res Lett* 2000;27:1195–8.
- [14] Hilfer R, Manwart C. Permeability and conductivity for reconstruction models of porous media. *Phys Rev E* 2001;64:021304.
- [15] Baruchel J, Buffière J-Y, Maire E, Merle P, Peix G. X-ray tomography in material science. Paris: Hermes; 2000.
- [16] Rolland Du Roscoat S, Bloch J-F, Thibault X. Synchrotron radiation microtomography applied to investigation of paper. *J Phys D: Appl Phys* 2005;38:A78–84.
- [17] Underwood EE. Quantitative stereology. Addison Wesley; 1969.
- [18] Serra J. Image analysis and mathematical morphology. London: Academic Press; 1982.
- [19] Delisee C, Jeulin D, Michaud F. Caractérisation morphologique et porosité en 3d de matériaux fibreux celluloseux. *CR Acad Sci* 2001;t. 329(série IIb):179–85.
- [20] Matheron G. *Éléments Pour Une Théorie Des Milieux Poreux*. Masson et Cie, 1967.
- [21] Jeulin D. Homogénéisation En Mécanique Des Matériaux. Hermes; 2001. p. 93 [chapter 4].